

Tandem photonic-crystal thin films surpassing Lambertian light-trapping limit over broad bandwidth and angular range

Ardavan Oskooi,^{a)} Yoshinori Tanaka, and Susumu Noda

Department of Electronic Science and Engineering, Kyoto University, Kyoto 615-8510, Japan

(Received 15 October 2013; accepted 21 February 2014; published online 5 March 2014)

Random surface texturing of an optically thick film to increase the path length of scattered light rays, first proposed nearly thirty years ago, has thus far remained the most effective approach for photon absorption over the widest set of conditions. Here, using recent advances in computational electrodynamics, we describe a general strategy for the design of a silicon thin film applicable to photovoltaic cells based on a quasi-resonant approach to light trapping where two partially disordered photonic-crystal slabs, stacked vertically on top of each other, have large absorption that surpasses the Lambertian limit over a broad bandwidth and angular range. © 2014 AIP Publishing LLC. [<http://dx.doi.org/10.1063/1.4867892>]

One of the fundamental issues underlying the design of silicon photovoltaic (PV) cells for use in realistic settings is the maximum absorption of incident sunlight over the widest possible range of wavelengths, polarizations, and angles using the thinnest material possible. While random or so-called Lambertian texturing of the surface to isotropically scatter incident light rays into a weakly absorbing thick film so as to increase the optical path length, as shown in Fig. 1(a), has thus far remained the most effective approach for light trapping over a wideband spectrum,^{1,2} recent thin-film nanostructured designs including photonic crystals (PCs)³ shown in Fig. 1(b) exploiting the more-complicated wave effects of photons have explored the possibility of superior performance^{4–18} but have been mainly limited to narrow bandwidths, select polarizations, or a restricted angular cone typical of delicate resonance-based phenomenon. The introduction of strong disorder, while improving robustness, nevertheless comes at the expense of light trapping relative to the unperturbed case.^{19,20} As a result, no proposal for a nanostructured silicon thin film capable of robust, super-Lambertian absorption over a large fraction of the solar spectrum has yet been made. While proposals for super-Lambertian absorption have been made for various other material systems,^{11,17} most have employed either slot-waveguide effects in unrealistically thin low-index absorbers, plasmonic phenomena using metals which tend to incur large losses or fictitious materials with wavelength-independent absorption coefficients that are not experimentally relevant. In this work, we present a different approach to light trapping made possible by recent advances in computational electrodynamics²¹ based on the quasi-resonant absorption of photons that combines the large absorption of optical resonances with the broadband and robust characteristics of disordered systems via a stacked arrangement of ordered PC slabs augmented with partial disorder that, for the first time using only silicon, surpasses by a wide margin the performance of an idealized Lambertian scatterer over a broad spectrum and angular cone.

Our tandem design, consisting of the same silicon film structured in two different ways and stacked vertically as

shown in Fig. 1(c), is the photonic analogue of the multi-junction cell that employs three or more *different* semiconductor films where the electronic bandgaps add complementarily to obtain wideband absorption. Here, we demonstrate the utility of a photonic approach, employing geometric structure alone that is more generally applicable to different fabrication methods through its design flexibility that involves applying any kind of partial disorder to any kind of photonic-crystal absorber, to enhance light trapping. This also offers improved performance but does not incur the constraints and limitations of optimally combining multiple material-specific electronic bandgaps as well as the significant fabrication challenges and costs of epitaxially growing films with mismatched atomic lattices on top of one another. We outline a two-part design strategy based on first maximizing, with a few-parameter gradient-free topology optimization, the number of resonant-absorption modes by using two crystalline-silicon PC slabs with a fixed total thickness of 1 μm stacked on top of each other such that their individual resonances add complementarily over the wideband spectrum, and then in the final step introducing a partial amount of disorder to both lattices to maximize the overall light trapping and boost robustness to go well beyond the Lambertian limit.

In our earlier work, we showed how individual resonant-absorption peaks of a thin-film PC slab can be broadened using partial disorder leading to an overall enhancement of the wideband absorption spectra.¹⁹ To understand quantitatively why disorder increases broadband light trapping in a PC, we use coupled-mode theory to derive an analytical expression for a single absorption resonance (at a frequency of ω_0) which has only one coupling channel for external light (a slight simplification which helps to make clear the role of disorder) in terms of the decay lifetimes (proportional to the quality factor) for radiation (τ_{rad}) and absorption (τ_{abs}) by the material³

$$A(\omega) = \frac{4}{\tau_{rad}\tau_{abs}} \cdot \frac{1}{(\omega - \omega_0)^2 + \left(\frac{1}{\tau_{rad}} + \frac{1}{\tau_{abs}}\right)^2}. \quad (1)$$

^{a)}Electronic mail: oskooi@qoe.kuee.kyoto-u.ac.jp

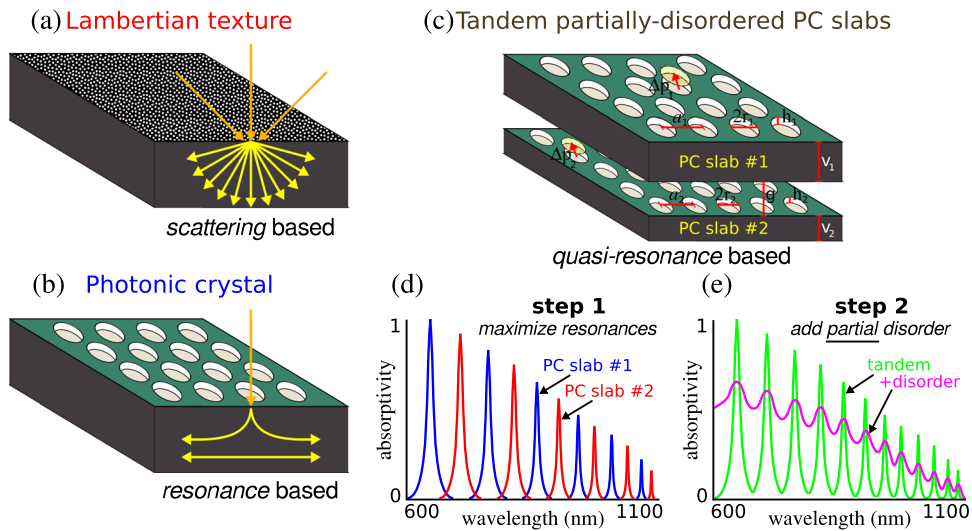


FIG. 1. (a) Random or so-called Lambertian texturing of the surface to isotropically scatter incident light rays into the plane of a weakly absorbing film so as to increase the optical path length. First proposed nearly 30 years ago, this has thus far remained the most effective approach for light trapping over the widest set of conditions. (b) Photonic-crystal slab and other nanostructured designs in which light trapping occurs by resonant absorption into a guided mode depend on delicate wave-interference effects and are thus intrinsically narrowband and restricted to a small angular cone. (c) Tandem arrangement of two PC slabs, both consisting of a square lattice of holes in silicon, stacked vertically on top of each other. Shown are the degrees of freedom—slab thicknesses v_1 and v_2 , lattice parameters a_1 and a_2 , hole radii r_1 and r_2 , hole heights h_1 and h_2 , and gap separation g —used in the topology optimization to (d) engineer as many non-overlapping resonances over the wideband solar spectrum as possible. Following this, (e) each hole is perturbed from its position in the unperturbed lattice by amounts Δp_1 (Δp_2) chosen randomly from a uniform distribution of values between 0 and $\overline{\Delta p_1}$ ($\overline{\Delta p_2}$) for both orthogonal in-plane directions of the top (bottom) slab to boost light trapping and robustness by creating a more-uniform absorption profile.

Broadband absorption for a thin-film PC design, consisting of a collection of such individual Lorentzian peaks, necessitates that we consider the *total* area spanned by Eq. (1) which is equivalent to its absorption cross section

$$\int_{-\infty}^{\infty} A(\omega) d\omega = \frac{4\pi}{\tau_{rad} + \tau_{abs}}. \quad (2)$$

The effect of disorder is to reduce the peak height but more importantly to broaden the peak width (proportional to $1/\tau_{rad} + 1/\tau_{abs}$) via primarily a *decrease* in τ_{rad} which therefore leads to an overall *increase* in broadband absorption from Eq. (2) (though τ_{abs} also changes with disorder due to variations in the nature of the guided mode, the change is much less pronounced than τ_{rad} mainly because the material absorption coefficient is fixed). Note that this analysis is only valid when coupling to a *resonant* Bloch mode which is why introducing too much disorder and eliminating the peaks altogether, thus transitioning to *non-resonant* Anderson-localized modes, results in sub-optimal light trapping.¹⁹

We consider the absorption of solar radiation in the wavelength regime spanning 600 nm to 1100 nm in which silicon is poorly absorbing and thus weak coupling to resonant Bloch modes of the PC most apparent. The overall light-trapping efficiency of each design can be quantified relative to an ideal perfect absorber which has unity absorptivity over the wavelength interval of interest by assuming that each absorbed photon with energy greater than the bandgap of silicon generates an exciton which contributes directly to the short-circuit current (this is equivalent to an internal quantum efficiency of 100%). This corresponds to the following definition of light-trapping efficiency

$$\frac{\int_{600nm}^{1100nm} \lambda \mathcal{I}(\lambda) \mathcal{A}(\lambda) d\lambda}{\int_{600nm}^{1100nm} \lambda \mathcal{I}(\lambda) d\lambda}, \quad (3)$$

where $\mathcal{I}(\lambda)$ is the terrestrial power density per unit wavelength from the sun at AM1.5²² and $\mathcal{A}(\lambda)$ is the absorptivity of the film.

The design strategy of maximizing the light-trapping efficiency by controllably introducing a partial amount of disorder to obtain just the right dose of peak broadening ultimately results in a more-uniform absorption profile where the absorptivity in the inter-peak regions is increased at the expense of the height of all peaks. This therefore suggests that in order to most effectively make use of partial disorder for light-trapping enhancement in a thin film the number of resonant modes must first be made *as large as possible* so that there is little bandwidth separation between peaks: by extending our previous slab design to include not one but *two* PC lattices stacked on top of one other and separated by a non-absorbing nanoscale gap layer, such that the absorption spectra of each lattice when combined adds complementarily (i.e., regions of low absorption in one lattice are compensated for by the high absorption of the other), the resonant-absorption characteristics of the PC augmented by partial disorder can potentially be exploited to the fullest extent possible for broadband absorption while also remaining feasible to large-scale industrial manufacturing. The low-index gap separation layer itself also provides additional mechanisms for light localization in nanostructured media that further contributes to enhancing absorption in the adjacent high-index layers while its effect on scattering-based

Lambertian-textured films is marginal. A schematic of this design approach, somewhat exaggerated for illustrative purposes, is shown in Figs. 1(d) and 1(e) in which the tandem structure is first optimized for *peak density* in the spectrum (which amounts to maximizing the number of non-overlapping resonant absorption modes of the two constituent PC lattices) and subsequently these narrow closely spaced resonances are slightly broadened with the addition of disorder to create a more-uniform absorption profile that is large in amplitude, broadband, and robust to incident radiation conditions. We consider here for simplicity the case of two PC slabs³ in vacuum separated by an air gap which both incorporates all essential physical phenomena and has direct applications to conventional thin-film PV cells in which individual layers including both high-index semiconductors and low-index transparent conductive oxides are grown by thin-film deposition tools.^{23,24} There is no need in the scope of the present work where the focus is solely on photon absorption in silicon to include an anti-reflection (AR) coating in the front or a perfect reflector in the back as would be customary in an actual PV cell, since the role of both components is mainly to enhance, oftentimes significantly,^{8,25} the absorption of *existing* resonances in the nanostructured films but not to give rise to new ones. Due to the complimentary way that the individual peaks of the two PCs combine in the tandem structure, a simple square lattice arrangement is adequate for good performance rendering unnecessary the need for intricate superlattice structures.^{11,18}

To perform the topology optimization, we combine the capabilities of Meep, a freely available open-source finite-difference time-domain (FDTD) tool,²⁶ to compute the absorption spectra at normal incidence with the nonlinear-optimization routines of NLOpt.^{27,28} Here, we need not consider absorption at off-normal incidence since the addition of disorder in the final step will automatically reduce the sensitivity to incident radiation conditions.¹⁹ Accurate topology optimization is made possible using Meep's subpixel averaging^{21,26,29} which also significantly reduces the size of the computation by lowering the minimum spatial resolution required for reliable results. This is important since the objective function is iterated over a large number of times to explore small changes to geometrical parameters in order to engineer as many absorption resonances over the wideband spectrum as possible which tend to be highly susceptible to numerical artifacts introduced by "staircased" features^{21,26,29} enabling FDTD to be used as a versatile 3D design optimization tool. We use intrinsic crystalline silicon as our absorbing material and incorporate its full broadband complex refractive index profile³⁰ into the FDTD simulations with accuracy even near its indirect bandgap of 1108 nm where absorption is almost negligible to obtain experimentally realistic results.²⁸ Although, for generality, modeling a tandem structure consisting of two completely independent PC slabs with arbitrary lattice constants is preferred, incorporating two distinct unit cells into a single 3D simulation is computationally impractical, yet this is a minor design limitation as the other six structural parameters—as shown in Fig. 1(c): the thickness of the top Si layer v_t (the bottom thickness v_b is known since the total thickness is fixed at $1\ \mu\text{m}$), the gap thickness g , the radius and height of the holes in the top and bottom

lattices r_t, h_t, r_b, h_b —provide sufficient flexibility for creating out-coupled Bloch-mode resonances over the entire range of the broadband solar spectrum. We also investigated the computationally tractable case of two PC slabs with lattice constants differing by a factor of two though the results were not found to be an improvement to the single lattice-constant design. A planewave source is incident from above onto the tandem structure and the absorption spectrum $\mathcal{A}(\lambda)$, equivalent to $1 - \text{reflection} - \text{transmission}$, is calculated by Fourier-transforming the response to a short pulse. The absorptivity threshold used by the objective function to count the total number of peaks in the spectrum is taken to be that of our baseline performance metric: an equivalent $1\ \mu\text{m}$ -thick Si film with Lambertian-textured surfaces^{2,31} which has an efficiency of 43.0% in our wavelength interval (computed using the same fitted material parameters as used in the simulations). Since resonances with especially large peak amplitudes contribute most to increasing the overall efficiency when broadened, we add an extra 30% to our absorptivity peak threshold at each wavelength which while making the problem more challenging gives rise to better results. We impose no restrictions on the peak width or spacing relative to other peaks although these could potentially be used for further refinement. Once an optimal set of parameters for the two-lattice structure is determined by running multiple times with different randomly chosen initial values to explore various local optima, we then form a supercell consisting of 10×10 unit cells of the optimal structure and add positional disorder to each unperturbed hole in both lattices (while ensuring no overlap between holes to conserve the filling fraction) by an amount Δp_1 (Δp_2) chosen randomly from a uniform distribution of values between 0 and $\overline{\Delta p_1}$ ($\overline{\Delta p_2}$) for both orthogonal in-plane directions for the top (bottom) slab. Three separate simulations are made for each structure and the results averaged due to the random nature of the design.

Figure 2(a) shows the absorptivity spectra for three thin-film designs each with a total crystalline-silicon thickness of $1\ \mu\text{m}$: an unpatterned film, a Lambertian-textured film [obtained from Eq. (1) of Ref. 31], and finally the topology-optimized tandem design consisting of two PC slabs (top: thickness 708 nm, hole radius 236 nm, hole height 260 nm and bottom: thickness 292 nm, hole radius 199 nm, hole height 244 nm) with a lattice parameter of 641 nm separated by a 228 nm gap. The tandem design has numerous narrow, high-amplitude peaks—signatures of the coherent-resonant Bloch modes—that span the entire broadband spectrum whereas the unpatterned slab has broad Fabry-Pérot resonances with low amplitude. The complimentary way that the resonances of the individual slabs combine to form the tandem structure can be seen in Figures 2(b) and 2(c), where the top slab accounts for most of the total number of peaks while the bottom slab contributes a few key resonances particularly at longer wavelengths. Note that while the Lambertian-textured slab has little and diminishing absorption at long wavelengths where the absorption coefficient of crystalline silicon is vanishingly small the PC design, due to its resonant nature, has large absorption albeit appearing only as very-narrow peaks (due to the rate-matching phenomena discussed previously that underlies the resonant coupling between radiation and absorption by the material, as silicon's absorption

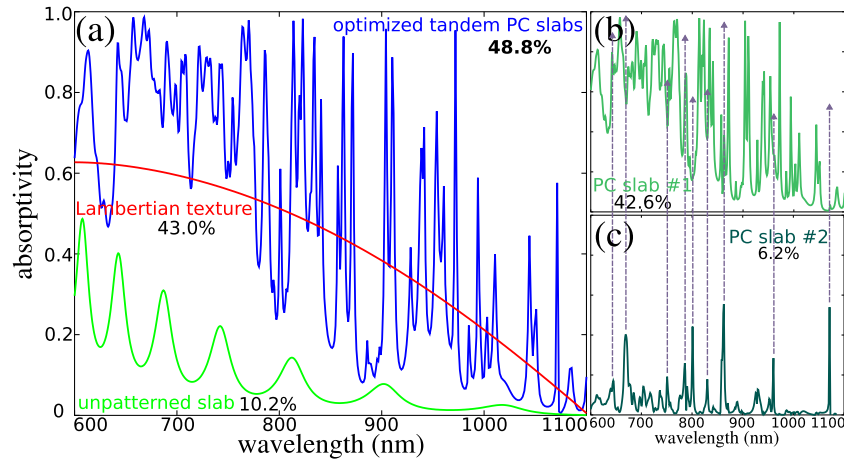


FIG. 2. (a) Absorption versus wavelength profile at normal incidence for three thin-film PV designs each with a total crystalline-silicon thickness of $1 \mu\text{m}$: an unpatterned slab (green), a Lambertian-textured slab (red) [obtained from Eq. (1) of Ref. 31] and the topology-optimized tandem PC slabs (blue). The tandem PC slabs both consist of a square lattice (periodicity, $a = 641 \text{ nm}$) of holes in silicon separated by a 228 nm gap. Shown for each design is the photon-absorption efficiency defined in Eq. (3) which is a measure of light trapping relative to a perfect absorber. (b) and (c) Individual absorption spectra for the top (slab #1: $v_t = 708 \text{ nm}$, $r_t = 236 \text{ nm}$, $h_t = 260 \text{ nm}$) and bottom (slab #2: $v_b = 292 \text{ nm}$, $r_b = 199 \text{ nm}$, $h_b = 244 \text{ nm}$) PC slabs of the optimized tandem design demonstrating how the resonances add complementarily over the broadband spectrum.

coefficient becomes smaller at larger wavelengths leading to a corresponding increase in τ_{abs} ,³ the total lifetime of the resonant mode τ_{tot} being $1/\tau_{tot} = 1/\tau_{abs} + 1/\tau_{rad}$ also increases resulting in the inversely proportional peak width generally becoming narrower which can be seen in Fig. 2). Nevertheless, the tandem design with its maximized peak density outperforms the Lambertian texture in light-trapping efficiency (48.8% versus 43.0%), although at off-normal angles and different polarizations of incident light the unperturbed lattices' resonance-based performance degrades significantly to below the Lambertian limit. Within the stacked arrangement, the efficiencies of the top and bottom slabs are 42.6% and 6.2%, respectively, while in isolation they are 37.9% and 22.3% highlighting in part the importance of inter-slab interactions to the overall absorption of the tandem design. For comparison, the optimized $1 \mu\text{m}$ -thick single-slab design (lattice parameter, hole radius and height of 640 nm , 256 nm , and 400 nm , respectively) produces seven fewer

resonances than the tandem design over the same wideband spectrum and therefore had a lower efficiency: nearly 5% below in absolute terms, yet still above the Lambertian limit.

By proceeding to controllably introduce a partial amount of disorder into the topology-optimized tandem design, we can simultaneously boost efficiency and improve robustness to exceed the Lambertian limit by an even wider margin over a large angular cone. Fig. 3(a) is a plot of the efficiency from Eq. (3) versus disorder for the optimized tandem-slabs and single-slab designs at normal incidence and shows that a positional disorder of approximately $\overline{\Delta p}_1 = \overline{\Delta p}_2 = 0.1a$ for the tandem slabs and $\overline{\Delta p} = 0.15a$ for the single slab results in maximal light trapping of 9.8% and 6.6% above the Lambertian limit, respectively, while additional disorder beyond these partial amounts leads to a steady decrease of the efficiency in line with the analysis presented earlier. The tandem design therefore is roughly twice as effective as the single slab in overcoming the Lambertian limit due mostly to

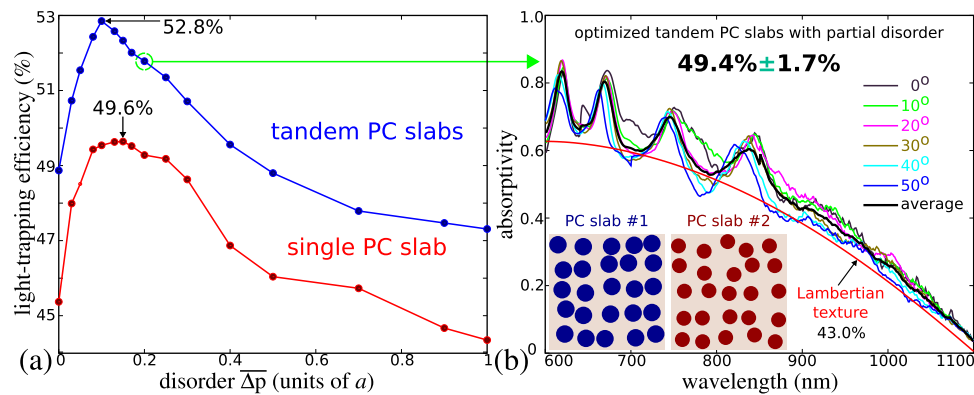


FIG. 3. (a) Light-trapping efficiency from Eq. (3) as computed from the absorption profile at normal incidence versus hole positional disorder for the topology-optimized tandem slabs (blue) and single slab (red) showing that partial disorder (tandem: $\overline{\Delta p}_1 = \overline{\Delta p}_2 = 0.1a$, single: $\overline{\Delta p} = 0.15a$) maximizes the light trapping (tandem: 52.8%, single: 49.6%) while additional disorder is sub optimal and leads to a steady decline. Note that the tandem design is nearly twice as effective as the single-slab design in surpassing the Lambertian limit. (b) Absorption versus wavelength profile at normal (0°) incidence and five off-normal (10° , 20° , 30° , 40° , 50°) angles of incidence averaged over both S and P polarizations of the optimized tandem design with the addition of partial disorder of $\overline{\Delta p}_1 = 0.2a$ and $\overline{\Delta p}_2 = 0.25a$ as shown in the inset schematics. The absorption profile for the individual angles are colored while the average of all the data which exceeds the Lambertian texture over the entire interval resulting in an overall light-trapping efficiency that is approximately 10% greater.

facilitating a larger number of absorption resonances. We quantify the performance robustness of each design as the standard deviation of the efficiency averaged over normal (0°) incidence and five off-normal (10° , 20° , 30° , 40° , 50°) angles of incidence for both S and P polarizations. A demonstration involving a larger angular range is possible but the necessary simulation times to ensure that the Fourier transforms used to compute the flux spectra have properly converged become prohibitively long. Since more disorder results in better robustness¹⁹ which is a key requirement of a practical solar cell we make a slight trade off and apply not the quantities which maximize efficiency at normal incidence in the tandem design but values slightly greater ($\overline{\Delta p_1} = 0.2a$ and $\overline{\Delta p_2} = 0.25a$) where the robustness is substantially larger: $49.5\% \pm 2.3\%$ for the former versus $49.4\% \pm 1.7\%$ for the latter. The average standard deviation in the efficiency computed over all sets of three separate random structures at each angle and polarization is nearly a factor of two less than that computed here indicating that the data are sufficiently converged. Fig. 3(b) demonstrates that the average performance of this tandem design has greater absorption than the Lambertian scatterer at every wavelength resulting in a light-trapping improvement of almost 10% above the Lambertian limit.

In summary, we have described a general design strategy for enhanced light trapping for a nanostructured silicon thin film. Our approach is based on the quasi-resonant absorption of photons in a tandem arrangement of partially disordered photonic-crystal slabs separated by a nanoscale gap. The overall light trapping surpasses a Lambertian-textured film by a wide margin over a large fraction of the solar spectrum and a broad angular cone.

This work was supported by Core Research for Evolutional Science and Technology (CREST) from the Japan Science and Technology Agency. A.O. was supported by a postdoctoral fellowship from the Japan Society for the Promotion of Science (JSPS).

¹E. Yablonovitch, *J. Opt. Soc. Am.* **72**(7), 899–907 (1982).

²E. Yablonovitch and G. D. Cody, *IEEE Trans. Electron Devices* **29**(2), 300–305 (1982).

³J. D. Joannopoulos, S. G. Johnson, R. D. Meade, and J. N. Winn, *Photonic Crystals: Molding the Flow of Light*, 2nd ed. (Princeton University Press, Princeton, NJ, 2008).

⁴D. Zhou and R. Biswas, *J. Appl. Phys.* **103**, 093102 (2008).

⁵A. Chutinan, N. P. Kherani, and S. Zukotynski, *Opt. Express* **17**(11), 8871–8878 (2009).

⁶Y. Park, E. Drouard, O. El Daif, X. Letarte, P. Viktorovitch, A. Fave, A. Kaminski, M. Lemiti, and C. Seassal, *Opt. Express* **17**(16), 14312–14321 (2009).

⁷E. Garnett and P. Yang, *Nano Lett.* **10**, 1082–1087 (2010).

⁸S. B. Mallick, M. Agrawal, and P. Peumans, *Opt. Express* **18**(6), 5691–5706 (2010).

⁹J. Zhu, Z. Yu, S. Fan, and Y. Cui, *Mater. Sci. Eng., R* **70**, 330–340 (2010).

¹⁰S. E. Han and G. Chen, *Nano Lett.* **10**, 4692–4696 (2010).

¹¹Z. Yu, A. Raman, and S. Fan, *Proc. Natl. Acad. Sci. U.S.A.* **107**(41), 17491–17496 (2010).

¹²S. Fahr, T. Kirchartz, C. Rockstuhl, and F. Lederer, *Opt. Express* **19**, A865–A874 (2011).

¹³X. Sheng, S. G. Johnson, J. Michel, and L. C. Kimerling, *Opt. Express* **19**, A841–A850 (2011).

¹⁴A. Bozzola, M. Liscidini, and L. C. Andreani, *Opt. Express* **20**, A224–244 (2012).

¹⁵K. X. Wang, Z. Yu, V. Liu, Y. Cui, and S. Fan, *Nano Lett.* **12**(3), 1616–1619 (2012).

¹⁶R. Biswas and C. Xu, *J. Non-Cryst. Solids* **358**, 2289–2294 (2012).

¹⁷J. N. Munday, D. M. Callahan, and H. A. Atwater, *Appl. Phys. Lett.* **100**, 121121 (2012).

¹⁸E. R. Martins, J. Li, Y. Liu, J. Zhou, and T. F. Krauss, *Phys. Rev. B* **86**, 041404 (2012).

¹⁹A. Oskooi, P. A. Favuzzi, Y. Tanaka, H. Shigeta, Y. Kawakami, and S. Noda, *Appl. Phys. Lett.* **100**, 181110 (2012).

²⁰K. Vynck, M. Buresi, F. Riboli, and D. S. Wiersma, *Nature Mater.* **11**, 1017–1022 (2012).

²¹A. Taflov, A. Oskooi, and S. G. Johnson, *Advances in FDTD Computational Electrodynamics: Photonics and Nanotechnology* (Artech House, 2013).

²²ASTMG173-03, Standard Tables for Reference Solar Spectral Irradiances: Direct Normal and Hemispherical on 37 degree Tilted Surface (ASTM International, West Conshohocken, PA, 2005).

²³R. Brendel, *Thin-Film Crystalline Silicon Solar Cells* (Wiley-VCH, Weinheim, Germany, 2003).

²⁴J. Poortmans and V. Arkhipov, *Thin Film Solar Cells: Fabrication, Characterization and Applications* (John Wiley & Sons, Ltd, 2006).

²⁵P. Bermel, C. Luo, L. Zeng, L. C. Kimerling, and J. D. Joannopoulos, *Opt. Express* **15**(25), 16986–17000 (2007).

²⁶A. F. Oskooi, D. Roundy, M. Ibanescu, P. Bermel, J. D. Joannopoulos, and S. G. Johnson, *Comput. Phys. Commun.* **181**, 687–702 (2010).

²⁷S. G. Johnson, The NLOpt Nonlinear Optimization Package, <http://ab-initio.mit.edu/nlopt>.

²⁸See supplementary material at <http://dx.doi.org/10.1063/1.4867892> for more details on the topology optimization and more details on how Si's material parameters were incorporated into the simulations.

²⁹A. Farjadpour, D. Roundy, A. Rodriguez, M. Ibanescu, P. Bermel, J. D. Joannopoulos, S. G. Johnson, and G. W. Burr, *Opt. Lett.* **31**, 2972–2974 (2006).

³⁰M. A. Green, *Sol. Energy Mater. Sol. Cells* **92**, 1305–1310 (2008).

³¹H. W. Deckman, C. B. Roxlo, and E. Yablonovitch, *Opt. Lett.* **8**(9), 491–493 (1983).

Tandem photonic-crystal thin films surpassing Lambertian light-trapping limit over broad bandwidth and angular range

Ardavan Oskooi,* Yoshinori Tanaka, and Susumu Noda

Department of Electronic Science & Engineering,

Kyoto University, Kyoto, 615-8510, Japan

* oskooi@qoe.kuee.kyoto-u.ac.jp

SUPPLEMENTAL ONLINE MATERIAL

A. Topology optimization using Meep and NLOpt

We combine the capabilities of our open-source finite-difference time-domain (FDTD) software tool Meep to compute the absorption spectra at normal incidence with the nonlinear optimization routines of NLOpt in order to maximize the number of resonant modes using topology optimization. Meep simulations consist of a 3d unit cell of the tandem structure at a resolution of 10 nanometers per pixel which in combination with the sub-pixel averaging can accurately model features down to a few nanometers. A Gaussian planewave source with a large temporal width coefficient to avoid an abrupt turn off is used to ensure a small amplitude for high-frequency components near the Nyquist frequency of the grid which have slow group velocities and thus are poorly absorbed by the perfectly-matched layers. The absorption spectra spanning 600nm to 1100nm is divided into 501 evenly-spaced frequency points and computed using the discrete-time Fourier transform of the fields at each frequency to obtain the reflection and transmission flux spectra from which absorption is derived. The simulation terminates when the absolute value squared of the fields has decayed by a factor of 10^{-8} from its maximum during the course of the entire simulation to ensure precision in the absorptivity data. To compute the absorption at off-normal angles of incidence, we use Bloch periodic boundary conditions with the same planewave source having a sinusoidal spatial profile and for improved accuracy divide the spectrum in half, compute both parts separately and combine them in post processing.

We use the BOBYQ gradient-free local optimization algorithm in NLOpt with the following parameters: a tolerance of 1 for the absolute change in the number of peaks of the objective function, a tolerance of 5nm for the absolute change of the geometrical parameters and a maximum iteration number of 50 (though in practice this is never reached). We first iterate over a large number of random initial values for the seven geometrical parameters and from this set choose those with the largest number of peaks to then maximize using the topology optimization.

A benefit to maximizing the number of resonant absorption modes is that it has a close correlation with the light-trapping efficiency as shown in Fig. 1 which is the key measure of device performance. Yet from the perspective of optimization where the choice of objective

function is critical (note that the tandem design has too many degrees of freedom for an exhaustive search of the design space), even though both tend to have a global optimum at identical co-ordinates the former with its more topographically-varying features and greater relative contrast between large and small values seems to be more suitable than the latter for enabling rapid exploration of a large number of local optima. This is particularly important since the gradient here is not known though adjoint methods [1] could potentially be used their implementation for such complex geometries presents significant overhead to the computation. Nevertheless, the number of resonant modes is a discrete quantity where changes can be readily discerned during a search of the parameter space while the efficiency, proportional to the area under the wideband absorption spectrum, undergoes less perceptible change with structure as seen in Fig. 1.

B. Accurately incorporating silicon’s material properties into Meep

Material absorption is modeled in Meep using a polarization field where physically the material dispersion (including loss) arises because the polarization of the material does not respond instantaneously to an applied field \mathbf{E} giving rise to $\mathbf{D} = \varepsilon_\infty \mathbf{E} + \mathbf{P}$, where ε_∞ is the instantaneous dielectric function and \mathbf{P} is the remaining frequency-dependent polarization density in the material. The polarization field itself is modeled using N -damped-harmonic oscillators, $\mathbf{P} = \sum_n \mathbf{P}_n$ such that the n -th polarization field is described by the following second-order partial differential equation which is discretized and then updated during each time step as an auxiliary field in the simulations:

$$\frac{d^2 \mathbf{P}_n}{dt^2} + \gamma_n \frac{d \mathbf{P}_n}{dt} + \omega_n^2 \mathbf{P}_n = \sigma_n(\mathbf{x}) \mathbf{E} \quad (1)$$

where ω_n is the resonance frequency, γ_n the decay rate and σ_n the strength of the absorption. This is equivalent to introducing a Lorentzian absorption resonance as an imaginary part of the permittivity function,

$$\varepsilon(\omega) = \varepsilon_\infty + \sum_n \frac{\sigma_n \omega_n^2}{\omega_n^2 - \omega^2 - i\omega \gamma_n}. \quad (2)$$

This formulation enables us in principle to accurately model any arbitrary, complex dielectric function using a nonlinear fit of the experimental data [2] similar to designing an

infinite impulse response (IIR) filter in signal processing but intrinsic crystalline silicon is particularly challenging since the absorption coefficient varies by nearly four orders of magnitude in the wavelength spectrum from 600nm to 1100nm and moreover the absorption coefficient is negligible (less than 10cm^{-1}) at long wavelengths due to silicon's indirect bandgap at 1108nm. To overcome this, it turns out that by introducing a slight amount of artificial numerical gain (while still keeping the material overall absorptive), equivalent to adding a $-i\kappa$ term (where $\kappa > 0$) to eq. (2), an accurate fit of the experimental data can be made using only a *single* Lorentzian resonance which has the added benefit that its impact on slowing down the time-stepping due to the auxiliary fields required is minimal. The role of the small gain is merely to reduce the absorption slightly at long wavelengths to enable better agreement with the experimental data; this is important since it is this regime where the effect of the broadened resonances of a PC lattice on enhancing light trapping relative to the Lambertian texture is most critical. We perform the nonlinear fit of the three-parameter Lorentzian (ω_1 , γ_1 and σ_1) and two additional variables (ε_∞ and κ) using the local gradient-based method of moving asymptotes algorithm of NLOpt and the comparison with the experimental data for both the real part of the refractive index and the absorption coefficient of silicon is shown in Fig. 2.

-
- [1] G. Strang, *Computational Science and Engineering* (Wellesley-Cambridge Press, Wellesley, MA, 2007).
- [2] M. Green, *Solar Energy Materials and Solar Cells* **92**, 1305 (2008).

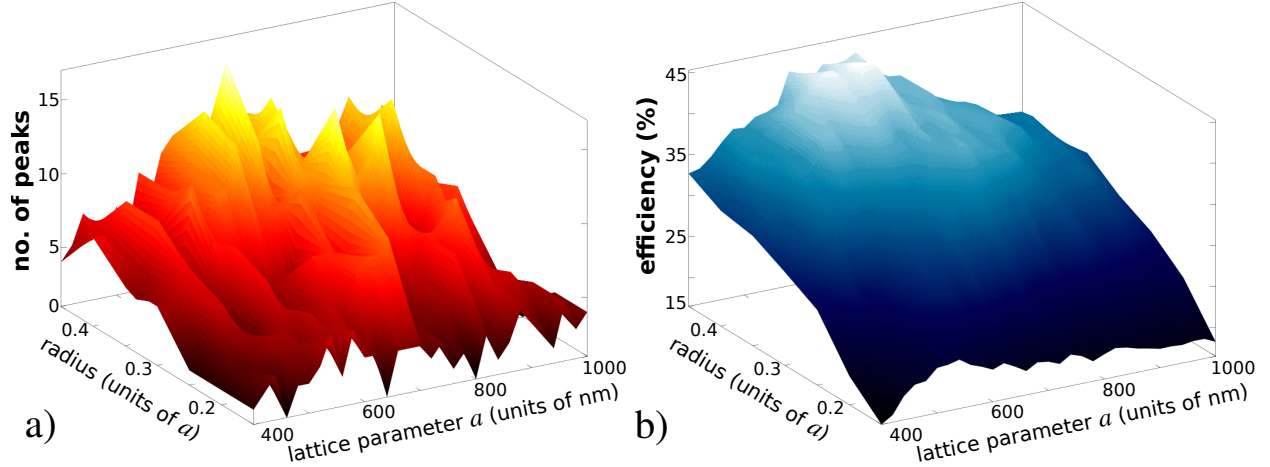


FIG. 1. A snapshot of two different parameter spaces corresponding to two objective functions – (a) the number of peaks or (b) the efficiency from eq. (3) of the main text – explored by the topology optimization when performing a gradient-free local search of a single PC slab with thickness of $1\mu\text{m}$ and a fixed hole depth of 400nm where the lattice parameter and hole radius are free parameters. Note the topographical resemblance between the two spaces as both have a global maximum at the same co-ordinate of $a=640\text{nm}$ and $r=0.4a$. The number of peaks though shows more finely-varying features and a greater relative contrast between large and small values (varying from a low of zero to a high of 17 while the efficiency range is only between 16.5% and 45.3%) making it easier to find extrema and thus a more suitable objective function for rapidly exploring many different local optima.

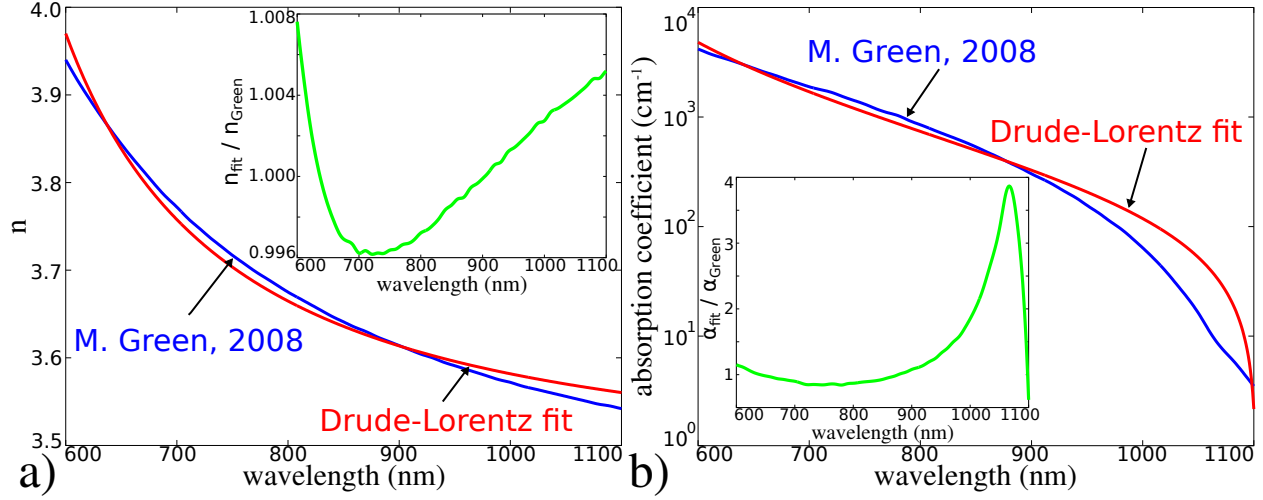


FIG. 2. A comparison between the experimental data for intrinsic crystalline silicon from Ref. 2 and a nonlinear numerical fit using the Drude-Lorentz model of eq. (2) supplemented with a small degree of artificial numerical gain for improved accuracy at long wavelengths. The real part of the refractive index is shown in (a) and the absorption coefficient in (b).